

# Optical and energy-loss spectra of MgO, ZnO, and CdO from *ab initio* many-body calculations

A. Schleife, C. Rödl, F. Fuchs, J. Furthmüller, and F. Bechstedt

*Institut für Festkörpertheorie und -optik, Friedrich-Schiller-Universität Jena, Max-Wien-Platz 1, 07743 Jena, Germany*  
*and European Theoretical Spectroscopy Facility, Max-Wien-Platz 1, 07743 Jena, Germany*

(Received 31 March 2009; revised manuscript received 17 June 2009; published 10 July 2009)

We compute optical properties including excitonic effects for the equilibrium polymorphs of three group-II metal monoxides by solving the Bethe-Salpeter equation. The underlying electronic structures are based on results of a recently developed *GW* approach starting from a hybrid exchange-correlation functional. The resulting quasiparticle band structures are discussed with respect to their mapping on computationally less expensive electronic structures computed using a *GGA+U* method together with a scissor operator  $\Delta$ . The efficiency of the latter approach allows the computation of real and imaginary parts of the dielectric function including excitonic effects up to photon energies of 32.5 eV with high accuracy. In addition, we derive the reflectivity as an optical key quantity as well as the energy-loss function. For dominant peak structures we identify the valence bands that mainly contribute to the corresponding transitions. Furthermore, the influence of excitonic effects and the comparison with results from other calculations and measurements are discussed in detail. Chemical trends across the oxides are identified.

DOI: [10.1103/PhysRevB.80.035112](https://doi.org/10.1103/PhysRevB.80.035112)

PACS number(s): 71.15.-m, 71.20.Nr, 71.35.Ee, 78.40.Fy

## I. INTRODUCTION

In recent years, there has been a renewed interest in various properties of group-II monoxides. This interest, especially in ZnO, is mainly driven by the industrial demand for optoelectronic devices operating in the deep blue or ultraviolet spectral region.<sup>1,2</sup> In addition, ZnO is environmentally friendly and even biocompatible. Its characteristics, especially when combined with the observed self-organized growth of a variety of nanostructures,<sup>3</sup> open a wide field of interesting physical effects and possible applications. This holds even more when ZnO is combined with other group-II oxides, such as MgO and CdO, in alloys and heterostructures. Mixed MgZnO crystals allow the widening of the energy gap of pure ZnO from 3.3 eV toward the ultraviolet spectral region.<sup>4,5</sup> In the visible spectral range, ternary CdZnO alloys are suitable candidates for optoelectronic devices.<sup>6</sup> Moreover, quantum well and other heterostructures, based on the combinations of MgZnO/ZnO and ZnO/CdZnO, allow a tailoring of electronic and optical properties by means of quantum-confinement effects.<sup>6-8</sup> Such combinations of the group-II oxides raise fundamental questions not only about the properties of ZnO but also, in particular, of the related materials, MgO and CdO.

While the electronic structure undoubtedly has large impact on the optical and electron-loss properties, unfortunately, the theoretical description of the band structure and electronic excitations of group-II metal compounds with anions from the first row of the Periodic Table is a challenge. The conventional quasiparticle (QP) approach based on the perturbation-theory treatment of the exchange-correlation (XC) self-energy<sup>9</sup> in Hedin's *GW* approximation<sup>10</sup> starting from a Kohn-Sham (KS) electronic structure<sup>11</sup> in local-density approximation or generalized-gradient approximation (GGA) fails. The resulting fundamental gap of wurtzite (wz)-ZnO is much too small<sup>12,13</sup> while rocksalt (rs)-CdO even exhibits a metallic ground state.<sup>14</sup> We solve these problems using a recently developed QP scheme<sup>12</sup> and predict QP

energy bands with high accuracy for the monoxides. The main drawback is that this QP scheme is extremely computer-time consuming. The corresponding electronic-structure calculations cannot be carried out for the large number of  $\mathbf{k}$  points which is required for the computation of the two-particle electron-hole pair Hamiltonian needed for the calculation of the frequency-dependent dielectric function including excitonic effects.<sup>15</sup> For that reason we project the results of the above-mentioned QP scheme onto such of a *GGA+U* method together with a scissor operator  $\Delta$  (see details in Refs. 15 and 16). We then are able to obtain the starting electronic structure for the solution of the Bethe-Salpeter equation (BSE), which allows for the accurate computation of the frequency-dependent dielectric function including excitonic and local-field effects (LFES) in a wide spectral range. It has been shown recently for ZnO (Ref. 17) that the many-body effects change the optical spectra significantly with respect to their description in the framework of independent Kohn-Sham particles.<sup>14</sup> In this paper we include a sufficient number of interband transitions to obtain converged results also for the real part of the dielectric function. Only an accurate description of real and imaginary parts up to high photon energies allows the derivation of the optical reflectivity or the electron-energy-loss spectra. We apply the currently best available methods to study these quantities and the chemical trend systematically along the row MgO, ZnO, and CdO on the same level of approximations.

After introducing the computational methods in Sec. II, we discuss the quality of the two different QP approaches by comparing the resulting band structures and densities of states (DOSs) in Sec. III. In Secs. IV and V we then present a systematic study of the optical properties, such as the dielectric function and the reflectivity, and also the electron-energy-loss function along the row MgO, ZnO, and CdO. Section VI concludes the paper.

## II. THEORETICAL AND COMPUTATIONAL METHODS

For a theoretical modeling of optical or electron-energy-loss properties by means of state-of-the-art *ab initio* calcula-

tions a thorough description of the dielectric function  $\varepsilon(\omega)$  is mandatory. It is the underlying key quantity to describe linear optical properties and allows the derivation of the reflectivity and the electron-energy-loss function. The precise computation of  $\varepsilon(\omega)$  up to high photon energies requires the solution of different problems. First of all, an adequate description of the underlying electronic structure is necessary. Second, the inclusion of excitonic and LFEs is, even though this is computationally expensive, inevitable. Approaches to both problems are elucidated in the following.

### A. QP band structure

A description of electronic structures including the excitation aspect requires the computation of QP wave functions and QP energy eigenvalues. One of the currently most reliable approaches to their computation for semiconductors or insulators is a two-step procedure:<sup>12</sup> first, energy eigenvalues and eigenfunctions of a generalized KS equation are computed using the HSE03 (Ref. 18) hybrid functional as zeroth approximation to the XC self-energy. In a second step, by applying Hedin's *GW* approximation<sup>10</sup> for the self-energy, QP energies are computed with an accuracy of about 0.1 eV.

The HSE03+*GW* approach has proven its reliability before, yielding results in convincing agreement with measurements for MgO,<sup>17</sup> ZnO,<sup>17,19</sup> and also CdO.<sup>17,20,21</sup> Despite a slight underestimation of the band gap of ZnO,<sup>12,13</sup> its band structure can be explained in accordance with experimental results by means of this scheme.<sup>19</sup> We also studied the direct and indirect gaps of CdO.<sup>21</sup> In addition, it has been demonstrated that the new approach gives excellent predictions for the DOS of occupied as well as empty bands of ZnO and CdO.<sup>19–21</sup>

However, such calculations that involve the spatially non-local HSE03 XC functional are computationally by far too expensive to be carried out for a large number of  $\mathbf{k}$  points as needed for the computation of an optical spectrum. Therefore, we follow a previously suggested procedure:<sup>15</sup> first, we compute *ab initio* QP band structures and DOS using the HSE03+*GW* approach. Second, we calculate wave functions on a significantly refined  $\mathbf{k}$ -point mesh using a semilocal GGA (Ref. 22) for XC, where we take into account an additional Coulomb repulsion  $U$  acting on the  $d$  shells of ZnO and CdO within the GGA+ $U$  method.<sup>23,24</sup> Finally, QP energies are computed by shifting these GGA+ $U$  eigenvalues of the conduction bands (CBs) by a scissor operator  $\Delta$ .<sup>9</sup> The two parameters  $U$  and  $\Delta$  are fixed in such a way that the band structures and DOS computed with the HSE03+*GW* and the GGA+ $U$ + $\Delta$  method show the best possible agreement, especially with respect to the fundamental gap and (for ZnO and CdO) the  $d$ -band positions. This approach, which is by far less computer-time consuming, indeed allows the inclusion of enough  $\mathbf{k}$  points and bands for the computation of optical properties up to high photon energies.

### B. Dielectric function

The macroscopic dielectric function is obtained by solving a BSE including the attractive screened electron-hole interaction and an exchange-like term accounting for LFEs.<sup>25,26</sup>

The BSE can be transformed to an eigenvalue problem for the excitonic electron-hole pair Hamiltonian whose solution determines the optical-absorption spectrum.<sup>27–29</sup>

One major drawback on the way of promoting such calculations toward convergence is the rapidly increasing computational effort. While the calculation of the high-energy part of the optical-absorption spectrum asks for the inclusion of a large number of CBs, the description of the fine structure of the absorption edge and low-energy optical transitions requires a fine  $\mathbf{k}$ -point sampling of the Brillouin zone (BZ) to converge bound exciton states.<sup>30</sup> The rank of the excitonic Hamiltonian is fixed by the number of pair states  $N = N_c \cdot N_v \cdot N_{\mathbf{k}}$ , with  $N_v$  as the number of valence bands (VBs),  $N_c$  as the number of CBs, and  $N_{\mathbf{k}}$  as the number of  $\mathbf{k}$  points. In our case  $N$  can easily amount to more than 50 000.

In order to present converged optical spectra for the entire spectral region and to account for the limited computer resources at the same time, we divide the problem of computing the dielectric function for a material into two separate problems for the low- and high-energy regions and correspondingly solve two BSEs. For the calculation of the low-energy part of the spectrum we sample the BZ with a very dense  $\mathbf{k}$  mesh, while for the inclusion of transitions up to photon energies of  $\hbar\omega = 32.5$  eV the  $\mathbf{k}$  sampling is reduced and the number of CBs is increased. The two resulting imaginary parts merge into each other smoothly. The real part of the dielectric function is connected to the imaginary part via a Kramers-Kronig relation. Therefore,  $\text{Re } \varepsilon(\omega)$  of the dielectric function describing the low-energy part of the spectrum is shifted by the difference of the static dielectric constants to match with  $\text{Re } \varepsilon(\omega)$  of the calculation reaching up to 32.5 eV.

To take also the contributions to the static dielectric constant into account which arise from transitions above 32.5 eV, we continue the absorption spectrum from 32.5 eV up to  $\approx 100$  eV within the independent-QP approximation.<sup>31</sup> This is well justified since the absolute value of the imaginary part is well below 10% of the peak values in this energy range and excitonic effects can safely be neglected.

Since MgO and ZnO are direct semiconductors, we are able to benefit from hybrid  $\mathbf{k}$ -point meshes, which have been shown to be very efficient for the computation of eigenvalues of individual excitonic bound states<sup>30</sup> as well as complete optical spectra.<sup>17</sup> For MgO, photon energies up to  $\hbar\omega = 13.4$  eV are included using a 10:5:30 hybrid mesh. This means (nomenclature explained in Ref. 30) that the whole BZ is sampled by a regular  $10 \times 10 \times 10$  Monkhorst-Pack (MP) mesh,<sup>32</sup> where the volume of the inner  $5 \times 5 \times 5$  boxes is filled by  $16 \times 16 \times 16$  MP points. That equals a density in the inner region that would require a  $30 \times 30 \times 30$  sampling of the whole BZ. For photon energies up to  $\hbar\omega = 32.5$  eV we use a regular  $10 \times 10 \times 10$  MP mesh for MgO. For ZnO, transitions up to 8.5 eV are computed using a hybrid  $8 \times 8 \times 6:5 \times 5 \times 5:20.8 \times 20.8 \times 15.6$  mesh and for the high-energy part we use regular  $6 \times 6 \times 4$  MP points. Because CdO is an indirect semiconductor,<sup>14,17</sup> it is not sufficient to sample only a certain region in  $\mathbf{k}$  space, e.g., around the  $\Gamma$  point, at higher density. Instead, we use two regular MP meshes:  $18 \times 18 \times 18$   $\mathbf{k}$  points for transitions up to 7.8 eV and  $8 \times 8 \times 8$  points up to an energy of 32.5 eV. Since all

these meshes are based on MP  $\mathbf{k}$  points, several high-symmetry points and high-symmetry lines are involved, naturally leading to a multitude of degenerate states. We shift the  $\mathbf{k}$  points by a small vector, which lies well inside one box of the coarse mesh in each case, in order to lift symmetry degeneracies and, therefore, accelerate the convergence of the respective optical quantities.

Despite this adaptive sampling of the BZ, the resulting exciton Hamiltonian matrices are still large. Hence, we use an efficient time-evolution scheme for the computation of the dielectric function<sup>33</sup> instead of a direct diagonalization of the excitonic Hamiltonian. This approach scales as  $\mathcal{O}(N^2)$  instead of  $\mathcal{O}(N^3)$  with  $N$  being the number of pair states.

For each material we study the equilibrium crystal structure, i.e., rs-MgO, wz-ZnO, and rs-CdO. The Vienna *Ab initio* Simulation Package (VASP) using the projector-augmented wave method<sup>34</sup> is applied for explicit calculations. The lattice parameters have been derived from a total-energy minimization before<sup>14</sup> and also the computational parameters are chosen as in Refs. 14 and 17. For rs-MgO and rs-CdO the  $\mathbf{k}$ -point sampling for the HSE03+*GW* QP band structure has been increased to  $16 \times 16 \times 16$  points in the BZ.

### III. QUASIPARTICLE BAND STRUCTURES

In Fig. 1 we show the QP band structures and DOS for (a) rs-MgO, (b) wz-ZnO, and (c) rs-CdO as obtained from the HSE03+*GW*, as well as the GGA+ $U+\Delta$ , approach. In addition, a selected number of QP eigenvalues at high-symmetry points of the BZ computed within the HSE03+*GW* approach are listed in Tables I–III for bands around the fundamental gaps. Corresponding differences of CB and VB energies give interband transition energies at high-symmetry points without the influence of excitonic and LFEs. For all three oxides the resulting single-QP DOSs show good agreement with spectra from photoemission spectroscopy, x-ray absorption, and resonant x-ray emission spectroscopy.<sup>17–21</sup> Small differences between our HSE03+*GW* calculations and experimental results have been discussed in these references. Here, we focus on the discussion of the GGA+ $U+\Delta$  approach since it is finally employed for the computation of the excitonic Hamiltonian and the optical properties. Therefore, we compare the quality of the QP eigenvalues computed within the GGA+ $U+\Delta$  approach to the benchmark HSE03+*GW* calculations in the following.

For MgO, density-functional theory (DFT) based on the semilocal GGA underestimates the fundamental direct gap at the  $\Gamma$  point by  $\Delta=2.99$  eV with respect to the HSE03+*GW* value of 7.49 eV. For ZnO (CdO), which include shallow *3d* (*4d*) electrons, the situation is more complicated since DFT-GGA severely underestimates the binding energies of the strongly localized cationic semicore *d* states.<sup>14</sup> We, therefore, include effective Coulomb repulsions  $U$  acting on the *d* levels with  $U=6.5$  eV for ZnO and  $U=4.5$  eV for CdO within the GGA+ $U$  approach.<sup>24</sup> As can be seen at energies around  $-6$  to  $-10$  eV in Figs. 1(b) and 1(c), these values are well suited to obtain good agreement for the respective bands and peaks in the VB DOS. However, we have to mention that the HSE03+*GW* description slightly

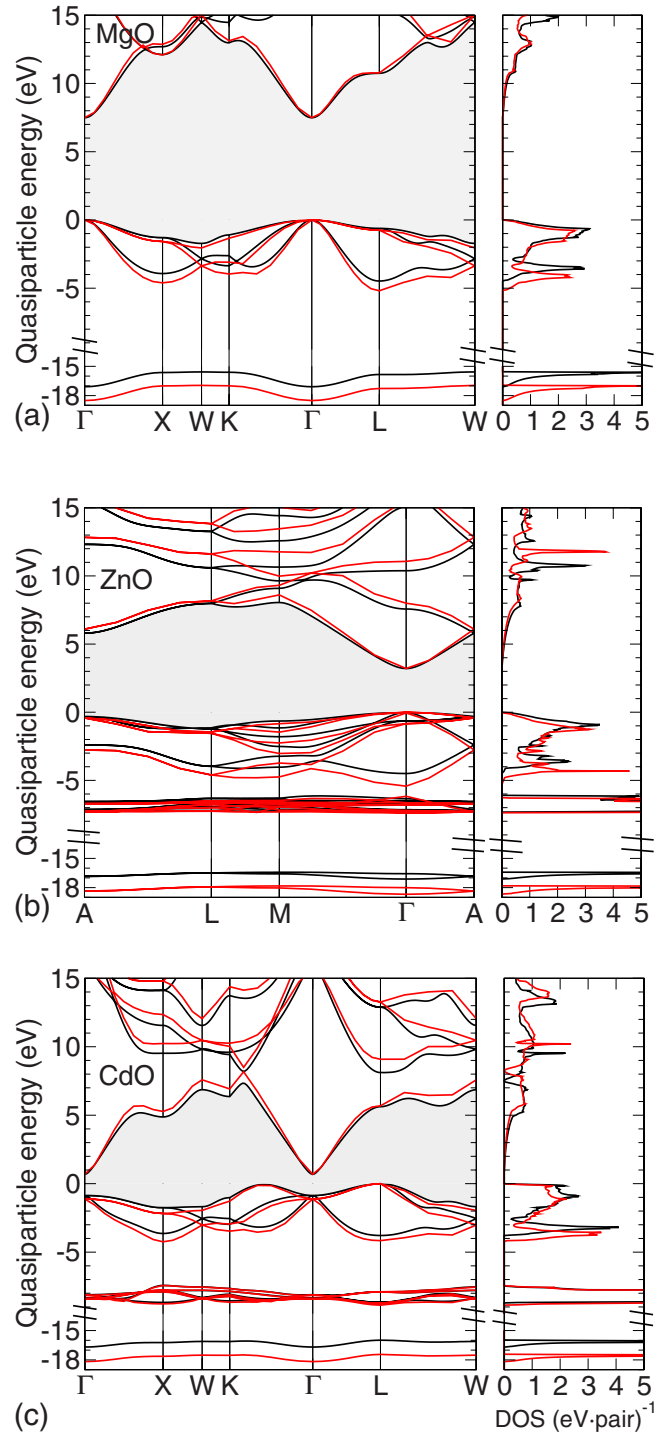


FIG. 1. (Color online) Quasiparticle band structures and densities of states of (a) rs-MgO, (b) wz-ZnO, and (c) rs-CdO calculated within the GGA+ $U+\Delta$  approach (black solid lines) and the HSE03+*GW* approach (red/bright solid lines). The VB maximum has been used as energy zero and the fundamental gap region is shaded.

underestimates the *d*-band binding energies with respect to the VB maximum in comparison to experimental results.<sup>17,19,20</sup> The remaining gap underestimation within the GGA+ $U$  approach is corrected by a scissor operator of  $\Delta=1.78$  eV ( $\Delta=1.07$  eV) to obtain the direct HSE03+*GW*

TABLE I. Quasiparticle eigenvalues of the lowest eight conduction (c1–c8) and highest four valence (v1–v4) bands of rs-MgO at high-symmetry points of the fcc BZ. All values in eV.

	c1	c2	c3	c4	c5	c6	c7	c8
$\Gamma$	7.49	19.05	19.05	19.05	21.94	25.16	25.16	27.47
$X$	12.08	12.87	16.78	22.41	22.41	29.02	30.95	34.32
$W$	15.04	15.04	15.39	18.61	25.16	25.16	30.27	33.09
$K$	13.13	15.01	16.09	21.45	21.50	28.18	31.14	32.26
$L$	10.77	16.34	19.44	19.44	23.73	25.90	25.90	31.66
	v4	v3	v2	v1				
$\Gamma$	-18.51	0.00	0.00	0.00				
$X$	-17.01	-4.61	-1.58	-1.58				
$W$	-16.95	-3.37	-3.36	-2.05				
$K$	-16.99	-3.96	-3.09	-1.34				
$L$	-17.27	-5.19	-0.74	-0.74				

gap of 3.21 eV (1.81 eV) for ZnO (CdO) (cf. also Tables I–III). In rs-CdO, an indirect gap of about 0.68 eV between the  $L_{3v}$  and the  $\Gamma_{1c}$  states occurs (cf. Table III), while the direct gap at  $\Gamma$  amounts to 1.81 eV. The calculated fundamental gaps  $E_g=7.49$ , 3.21, and 0.68 eV for rs-MgO, wz-ZnO, and rs-CdO, respectively, only slightly underestimate the experimental values 7.67, 3.44, and 0.84 eV.<sup>35</sup> One reason for the observed deviation is the atomic geometry obtained from the DFT-GGA approach, which tends to overestimate the lattice constants slightly and, hence, gives too small gaps.

For all three oxides, the bandwidth of the uppermost O  $2p$ -derived VBs obtained within the GGA+ $U$ + $\Delta$  approach is underestimated by about 0.5 eV with respect to the HSE03+ $GW$  results, while the binding energy of the O  $2s$  electrons is underestimated by about 1.4 eV using the GGA+ $U$ + $\Delta$  approach. The too small O  $2p$  bandwidth slightly affects the optical properties in the low-energy range, i.e., the lowest VB-CB transitions. The influence of the underestimated O  $2s$  binding energy in the high-photon-energy region above  $\hbar\omega=16$  eV remains small because of the low

oscillator strengths for the corresponding high-energy optical transitions.

In summary, Fig. 1 clearly shows that the differences between the QP eigenvalues from the GGA+ $U$ + $\Delta$  approach and the HSE03+ $GW$  approach are small on the considered energy scale. We observe the general trend that the GGA+ $U$ + $\Delta$  method computes the higher-lying CBs slightly too low in energy. Nevertheless, the overall agreement in Fig. 1 is sufficient; therefore, the GGA+ $U$ + $\Delta$  scheme seems reasonably justified to generate the starting electronic structure for the optical calculations in a wide range of photon energies.<sup>15</sup> We emphasize that the parameters  $U$  and  $\Delta$  are not empirically chosen but have been obtained from a comparison to the *ab initio* HSE03+ $GW$  approach, which itself agrees well with experimental results.

#### IV. DIELECTRIC FUNCTION

In Fig. 2 we present the computed results for the real and imaginary parts of the frequency-dependent macroscopic dielectric function  $\epsilon(\omega)$  for the three oxides up to energies of

TABLE II. Quasiparticle eigenvalues of the lowest eight conduction (c1–c8) and highest eight valence (v1–v8) bands of wz-ZnO at high-symmetry points of the hexagonal BZ. All values in eV.

	c1	c2	c3	c4	c5	c6	c7	c8
$\Gamma$	3.21	8.00	11.07	15.60	15.60	16.66	17.02	17.02
$A$	6.10	6.10	12.83	12.83	15.91	15.91	15.91	15.91
$L$	8.17	8.17	11.62	11.62	13.83	13.83	16.48	16.48
$M$	8.61	9.31	9.99	11.77	13.46	15.03	15.79	17.15
	v8	v7	v6	v5	v4	v3	v2	v1
$\Gamma$	-6.65	-6.65	-5.43	-0.84	-0.84	-0.05	0.00	0.00
$A$	-6.71	-6.71	-2.77	-2.77	-0.42	-0.42	-0.42	-0.42
$L$	-6.52	-6.52	-4.60	-4.60	-1.55	-1.55	-1.45	-1.45
$M$	-6.60	-6.47	-4.75	-3.73	-3.03	-2.26	-1.46	-0.84

TABLE III. Quasiparticle eigenvalues of the lowest eight conduction (c1–c8) and highest nine valence (v1–v9) bands of rs-CdO at high-symmetry points of the fcc BZ. All values in eV.

	c1	c2	c3	c4	c5	c6	c7	c8	
$\Gamma$	0.68	15.63	18.23	18.23	18.23	19.40	19.40	19.40	
$X$	5.27	10.24	12.36	14.81	14.81	24.80	25.99	28.88	
$W$	7.58	10.47	10.47	12.05	19.78	19.78	27.26	27.69	
$K$	6.92	10.03	10.26	14.38	16.84	22.70	25.71	27.08	
$L$	5.69	9.09	13.27	13.27	18.81	22.04	23.31	23.31	
	v9	v8	v7	v6	v5	v4	v3	v2	v1
$\Gamma$	-18.17	-8.40	-8.40	-8.40	-8.15	-8.15	-1.12	-1.12	-1.12
$X$	-17.63	-8.78	-7.90	-7.78	-7.77	-7.43	-4.25	-2.18	-2.18
$W$	-17.52	-8.41	-8.41	-8.36	-7.77	-7.55	-3.02	-3.02	-1.95
$K$	-17.53	-8.66	-8.24	-8.11	-7.86	-7.67	-3.47	-2.95	-1.27
$L$	-17.44	-8.87	-8.74	-8.74	-7.90	-7.90	-4.16	0	0

32.5 eV. A Lorentzian broadening of 0.1 eV has been used in all cases. Comparison with available experimental spectra obtained by means of spectroscopic ellipsometry<sup>36,37</sup> and Kramers-Kronig analysis of reflectance data<sup>38</sup> is given. Due to the hexagonal crystal symmetry of wz-ZnO, we distinguish between ordinary light polarization [ $\mathbf{E}$  perpendicular ( $\perp$ ) to the  $c$  axis of the hexagonal crystal] and extraordinary light polarization [ $\mathbf{E}$  parallel ( $\parallel$ ) to the  $c$  axis].

Using a computationally less expensive approach, in Ref. 14 the dielectric functions of MgO, ZnO, and CdO are calculated within the independent particle or random-phase approximation (RPA) and the Ehrenreich-Cohen formula<sup>39</sup> using KS eigenvalues and wave functions obtained with GGA as approximation to XC. Substituting the KS eigenvalues by the QP energies obtained within the GGA+ $U+\Delta$  method yields the independent-QP approximation and results in a blueshift of the absorption spectrum by 1–3 eV for the oxides studied here (see Sec. III). The inclusion of excitonic and LFEs in summary leads to a redshift with respect to the independent-QP spectrum, but it does not compensate the preceding blueshift. Thus, a blueshift of about 1–2 eV compared to the DFT-GGA results<sup>14</sup> remains. Furthermore, the excitonic effects cause a redistribution of spectral strength toward lower photon energies leading to a Coulomb enhancement of the peak intensities or Plateau heights by up to 60%. This effect is largest for MgO and less pronounced for ZnO and CdO, according to the increasing screening constants.

First of all, the inclusion of many-body effects ameliorates the values for the macroscopic static electronic dielectric constants  $\epsilon_{\infty} = \text{Re } \epsilon(\omega=0)$  (cf. Table IV). While for MgO, ZnO, and CdO they are overestimated within RPA,<sup>14</sup> we now observe improved agreement with experimental results. For rs-MgO we obtain  $\epsilon_{\infty} = 3.12$  in good agreement with the measured value of  $\epsilon_{\infty} = 2.94$ .<sup>35</sup> In the case of wz-ZnO, we find values  $\epsilon_{\infty}^{\parallel} = 4.08$  and  $\epsilon_{\infty}^{\perp} = 4.01$  only slightly larger than the experimental findings  $\epsilon_{\infty}^{\parallel} = 3.75$  and  $\epsilon_{\infty}^{\perp} = 3.70$ .<sup>35</sup> For rs-CdO we predict a dielectric constant of  $\epsilon_{\infty} = 6.07$  in comparison with values  $\epsilon_{\infty} = 3.80, \dots, 7.02$  derived from refractive index

data.<sup>35</sup> Going from MgO over ZnO to CdO, the screening constants increase as the fundamental gaps decrease.

As can be seen in Fig. 2 the substantial optical absorption for all materials is restricted to photon energies below  $\hbar\omega \approx 25$  eV. In more detail, for MgO we find a pronounced peak in the imaginary part of the dielectric function close to the absorption edge [peak E in Fig. 2(a)]. It originates from a bound Wannier-Mott-like excitonic state, which has been studied in detail elsewhere.<sup>30</sup> For peaks beyond the absorption-edge tests on the RPA level have shown that it is difficult to clearly assign them to van Hove singularities in the band structure as done before.<sup>40</sup> In addition, the Coulomb interaction introduces a coupling of VB and CB states from different  $\mathbf{k}$  points. This Coulomb-induced mixing renders it even less feasible to point out special high-symmetry  $\mathbf{k}$  points as origin for certain spectral features. Instead, the peaks consist of contributions from the entire  $\mathbf{k}$  space for the materials studied here. For that reason we discuss the three remarkable peaks above the absorption edge in the spectrum by assigning them to peaks in the RPA spectrum:<sup>14</sup> peak A at  $\hbar\omega \approx 10$  eV originates mainly from transitions between the two highest VBs and the CBs while the second one (B) at  $\hbar\omega \approx 13$  eV is caused almost completely by transitions from the uppermost VB into the CBs. Finally, peak C near  $\hbar\omega = 16$  eV is almost equally composed of transitions from all three O  $2p$  VBs into the CBs, with the second and third VBs contributing slightly more than the first. Peaks A and B are almost invisible as distinct peaks in the joint DOS. The formation of all three peaks is strongly influenced by the corresponding optical transition-matrix elements (for a definition see Ref. 41).

Regarding the energetic positions of the peaks, the agreement with the measured imaginary part<sup>37</sup> is almost perfect [see Fig. 2(a)]. This also holds for other measured spectra<sup>42,43</sup> with slightly varying peak positions and intensities. There are intensity deviations, which may be partly related to a larger lifetime and instrumental broadening for transitions with final states above the vacuum level. In any case, due to the good convergence of our calculations, the

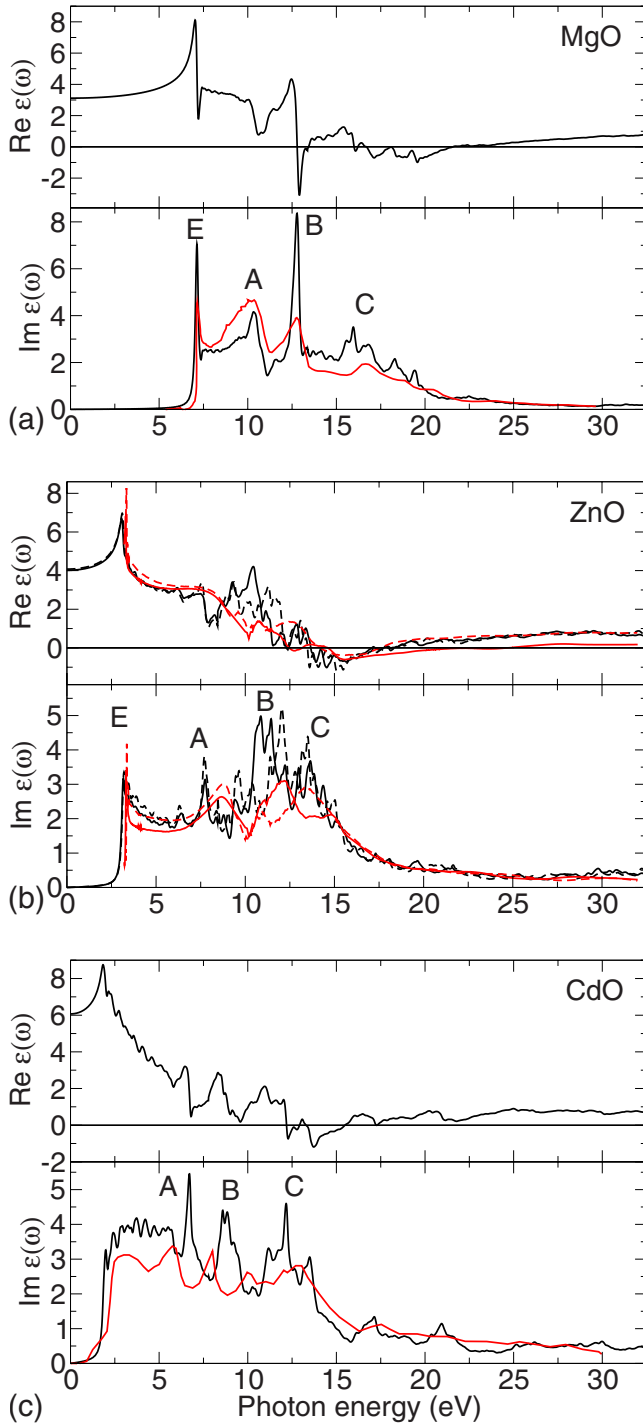


FIG. 2. (Color online) Real and imaginary parts of the dielectric function of (a) rs-MgO, (b) wz-ZnO, and (c) rs-CdO including excitonic effects (black curves). We compare to experimental (red/bright lines) results from Ref. 37 (MgO), Ref. 36 (ZnO), and Ref. 38 (CdO). For the hexagonal wz-ZnO curves for ordinary light polarization (solid lines) as well as for extraordinary polarization (dashed lines) are shown.

agreement with respect to peak positions as well as peak heights is much better than found in previous calculations also including excitonic effects.<sup>28,44</sup>

TABLE IV. Macroscopic static electronic dielectric constants.

	rs-MgO	wz-ZnO	rs-CdO
BSE	3.12	4.08(∥), 4.01(⊥)	6.07
Expt. <sup>a</sup>	2.94	3.75(∥), 3.70(⊥)	3.80, ..., 7.02

<sup>a</sup>Reference 35.

In Fig. 2(b) it can be seen that also the absorption edge of ZnO is dominated by bound excitonic states (peak E). These Wannier-Mott-like excitons have been studied before in detail.<sup>45,46</sup> Independent of the light polarization, we assign three main spectral features above the excitonic peak in the imaginary part of the dielectric function to corresponding peaks in the RPA spectrum of wz-ZnO. Structure A at around  $\hbar\omega = 7.7$  eV originates mostly from transitions from the uppermost four VBs into CB states. While the peak complex B between 10 and 15 eV is mainly caused by transitions from all O  $2p$  VBs into the CBs, its low-energy part directly above  $\hbar\omega = 10$  eV is dominated by transitions from the third and fourth VBs. Excitonic and transition-matrix-element effects significantly modify these peak structures in comparison to the peaks in the joint DOS. Furthermore, above  $\hbar\omega \approx 10$  eV the accumulated contribution of transitions from all Zn  $3d$ -related bands is comparable to the contribution of each O  $2p$  band. Above  $\hbar\omega \approx 20$  eV, the overall contribution of transitions from Zn  $3d$  states varies even between 20% and 50%. In addition, the small structure at around  $\hbar\omega \approx 20$  eV in the computed spectrum can be attributed to transitions from the  $d$  bands into higher  $p$ -type CBs.

Another interesting aspect is the optical anisotropy caused by the hexagonal crystal structure of wz-ZnO. This polarization anisotropy is relatively weak in the plateaulike region up to  $\hbar\omega \approx 8$  eV. It is much more pronounced in the narrow energy region around the band-edge excitons<sup>45</sup> and also for energies of about 10–14 eV. The uppermost three O  $2p$  VBs contribute most to this anisotropy. While transitions from the third VB cause the large contributions between  $\approx 10$  and 11.5 eV for perpendicular polarization, transitions mainly from the first and second VBs form the peaks for parallel polarization between 12 and 14 eV.

Compared to experimental curves<sup>36</sup> for the imaginary and real parts of the dielectric function, we find that we slightly overestimate the plateau height in the energy region  $\hbar\omega = 4$ –7 eV. Furthermore, we underestimate the energetic position of a peak around 8.9 eV in experiment by about 1 eV. While the first discrepancy may be an artifact of the surface-layer corrections used in the description of the ellipsometry measurements, we attribute the differences in the peak positions to having merely used a scissor operator  $\Delta$  for QP corrections. As discussed in Sec. III, the scissor approach typically underestimates the QP shifts for higher-lying CBs, which explains why we may underestimate the energetic positions of the associated absorption peaks. Nevertheless, peaks corresponding to each other in measured and calculated spectra can be clearly assigned. The overall agreement between experiment and theory in the high-energy region above  $\hbar\omega \approx 15$  eV is much better. This holds for both the

absolute values of real and imaginary parts as well as their frequency variations. Also the optical anisotropy with respect to the light polarization in the energy region of higher optical transitions agrees excellently with experimental findings.<sup>40,47</sup> A previous computation including excitonic effects<sup>46</sup> shows less agreement for the excitonic peak close to the absorption edge as well as the plateau region which we believe is due to convergence issues. In general, an important reason for deviations between experimental and theoretical results regarding peak positions or the optical anisotropy is a possible strain in the sample. Test calculations have shown that a compressive strain of about 2% has a noticeable influence on the optical anisotropy in wz-ZnO.

Contrary to the direct-gap semiconductors rs-MgO and wz-ZnO, the indirect rs-CdO does not show excitonic bound states below the absorption edge [see Fig. 2(c)]. Nevertheless, important features already observed for rs-MgO also appear in the case of CdO, especially in the high-frequency region. Above the absorption onset, a plateaulike region up to  $\hbar\omega=6$  eV appears in the imaginary part. Higher in energy we find again three remarkable peak structures and assign them to the corresponding peaks in the RPA spectrum. From this analysis we find that peak A at  $\hbar\omega=6.7$  eV originates mostly from transitions from the topmost VB into the CBs. The second peak (B) at  $\hbar\omega\approx 8.8$  eV consists of almost equal contributions from the three O 2p VBs. The peak complex C between 11 and 13 eV is dominated by contributions from the uppermost two VBs and can also be related to a high joint DOS. Such an identification is very difficult for the first two peaks in this energy region since their enhancement is mainly due to oscillator-strength effects. As in the case of wz-ZnO, the contributions of the Cd 4d states become more important above  $\hbar\omega\approx 12$  eV because strong Cd 5p contributions to the CB wave functions are necessary for large optical-matrix elements. Transitions from the d states are the origin of the two peaks around  $\hbar\omega=17$  eV and  $\hbar\omega=21$  eV.

In Fig. 2(c) we compare to an experimental curve that Freeouf<sup>38</sup> obtained by Kramers-Kronig analysis. For the low-energy region up to approximately 6 eV and also for energies higher than  $\approx 15$  eV the agreement is good. As for MgO and ZnO, also for CdO we seemingly underestimate the energetic positions of the three distinct spectral structures in the energy region between 6 and 15 eV by about 1 and 2 eV. This can be attributed either to the quality of the samples or to the use of a scissor operator in our calculations, as explained before. Nevertheless, even though for all the oxides the absolute values of the dielectric function are relatively small, we obtain a remarkably good agreement of our calculated results with experimental findings.

Comparing the three dielectric functions in Fig. 2 for the studied oxides, also chemical trends can be identified. For all the oxides we find a three-peak structure (see peaks A–C in Fig. 2) in the imaginary part of the dielectric function. This feature occurs even for wz-ZnO despite the different crystal structure. In comparison to MgO, the peaks occur at lower energies of about 7–15 eV for ZnO and 6–14 eV for CdO. Even the relative peak heights follow a chemical trend. While for MgO peak B is clearly the largest, its relative height decreases going to ZnO. In CdO peak B is the smallest one of A–C.

## V. REFLECTIVITY AND ENERGY LOSS

The macroscopic dielectric function  $\varepsilon(\omega)$  as discussed above allows the derivation of all linear optical quantities and of the electron-energy-loss function in the limit of vanishing transferred momenta. First, we focus our attention to the Fresnel reflectivity  $R(\omega)$  for normal incidence

$$R(\omega) = \left| \frac{\sqrt{\varepsilon(\omega)} - 1}{\sqrt{\varepsilon(\omega)} + 1} \right|^2 \quad (1)$$

with the complex dielectric function  $\varepsilon(\omega)$  and the photon energy  $\hbar\omega$ . Neglecting retardation and surface effects, the electron-energy-loss function  $-\text{Im} \varepsilon^{-1}(\omega)$  is given by

$$-\text{Im} \varepsilon^{-1}(\omega) = \frac{\text{Im} \varepsilon(\omega)}{[\text{Re} \varepsilon(\omega)]^2 + [\text{Im} \varepsilon(\omega)]^2} \quad (2)$$

with  $\hbar\omega$  as the loss energy. In the case of wz-ZnO, we again distinguish between  $\parallel$  and  $\perp$  quantities and follow the previously introduced definition.

### A. Reflectivities

In Fig. 3(a) we plot the reflectivity for rs-MgO as computed according to Eq. (1) from  $\varepsilon(\omega)$  in Fig. 2. Above the peak near 7.2 eV caused by the excitonic absorption a plateaulike frequency dependence follows. The peaks at  $\hbar\omega = 11$  and 13 eV in the reflectivity curve are clearly related to peaks in the dielectric function [cf. Fig. 2(a)], i.e., to interband transitions modified by excitonic effects. At higher energies we find one sharp and three broader peaks of strong reflectivity. From investigating the origin of the corresponding peaks in the RPA dielectric function we conclude that they are due to interband transitions of varying strength from the O 2p VBs. The comparison shows good agreement with an experimental curve<sup>37</sup> regarding the energetic positions of the peaks. In the measurement the peaks occur about 0.3 eV higher in energy while the overall structure is reproduced very well. Even the three-peak structure of the calculated reflectivity between  $\hbar\omega\approx 16.5$  eV and  $\hbar\omega\approx 21.5$  eV agrees with the experimental result. In the energy range  $\hbar\omega < 15$  eV the intensities, especially between the peaks, match well. In the high-energy range we overestimate the measured reflectivity. One reason for these deviations might be the sample quality.

In Fig. 3(b) we show the reflectivity curves for wz-ZnO. The pronounced peak caused by the excitonic absorption occurs at around 3.2 eV, i.e., about 0.1 eV below its experimental position due to the underestimation of the QP gap (cf. Table II). As already found for MgO and also for ZnO the reflectivity peaks up to 13.5 eV can be easily related to the peak structure of the imaginary part of the dielectric function in Fig. 2(b). In addition, the broad spectral structure between 14 and 17 eV may be traced back to a valleylike behavior of the real part. Since both real parts  $\text{Re} \varepsilon^{\parallel}(\omega)$  and  $\text{Re} \varepsilon^{\perp}(\omega)$  are close to zero in this energy regime, the reflectivity is significantly enhanced. The reflectivity peak near  $\hbar\omega\approx 20$  eV is caused by the absorption peak which we have related to transitions from Zn 3d states into CBs. Up to photon energies of  $\hbar\omega\approx 10$  eV (except of the excitonic peak) the anisotropy

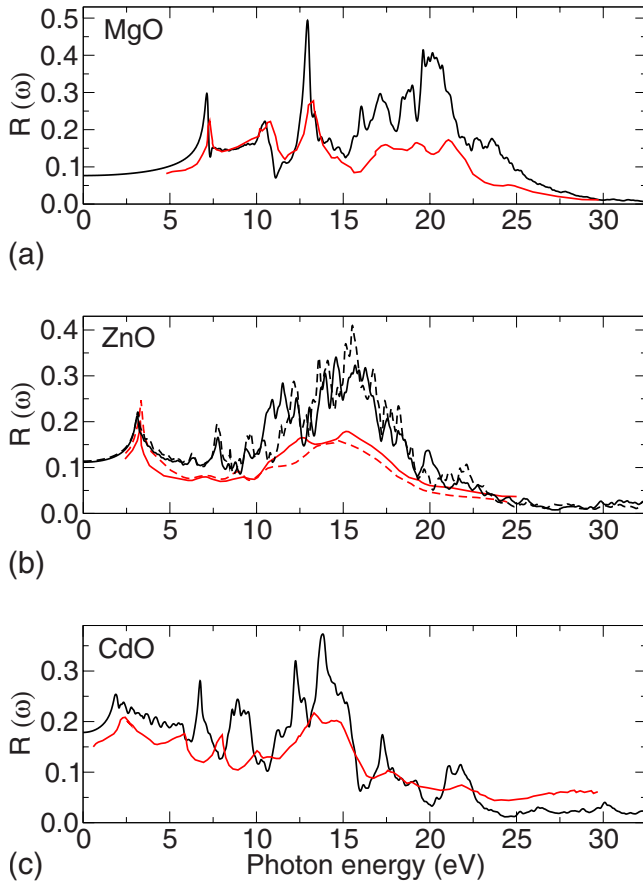


FIG. 3. (Color online) Reflectivity  $R(\omega)$  according to Eq. (1) of (a) rs-MgO, (b) wz-ZnO, and (c) rs-CdO including excitonic effects (black curves). We compare to experimental (red/bright lines) results from Ref. 37 (MgO), Ref. 47 (ZnO), and Ref. 38 (CdO). For the hexagonal wz-ZnO curves for ordinary polarization (solid lines) as well as for extraordinary polarization (dashed lines) are shown.

due to the hexagonal wz lattice structure is rather small. At higher energies, there is one peak at around  $\hbar\omega=11$  eV, which only occurs for ordinary polarization. On the other hand, the peak near  $\hbar\omega=15.5$  eV is more pronounced for extraordinary polarization. Compared to the measured reflectivities,<sup>38,47</sup> we observe that the general line shapes agree well. However, the theoretical spectra exhibit much more fine structure and, moreover, more pronounced peaks. Again, this discrepancy might be related to the sample quality, especially the overestimation of the reflectivity in the energy range of 5–20 eV. If we increase the effective broadening to values larger than 0.1 eV accounting for larger lifetime and instrumental broadening, the fine structure, but not the general peak structure, almost disappears. Hence, the agreement improves. Another possible reason for the overestimation of the reflectivity in the high-energy region may be the surface roughness of the samples. This leads to diffuse scattering becoming increasingly strong at higher frequencies as pointed out by Lambrecht *et al.*<sup>48,49</sup>

The computed result for the reflectivity of rs-CdO is shown in Fig. 2(c). For this material the reflectivity curve shows five distinctive peak complexes which can be easily related to corresponding structures in the real and imaginary

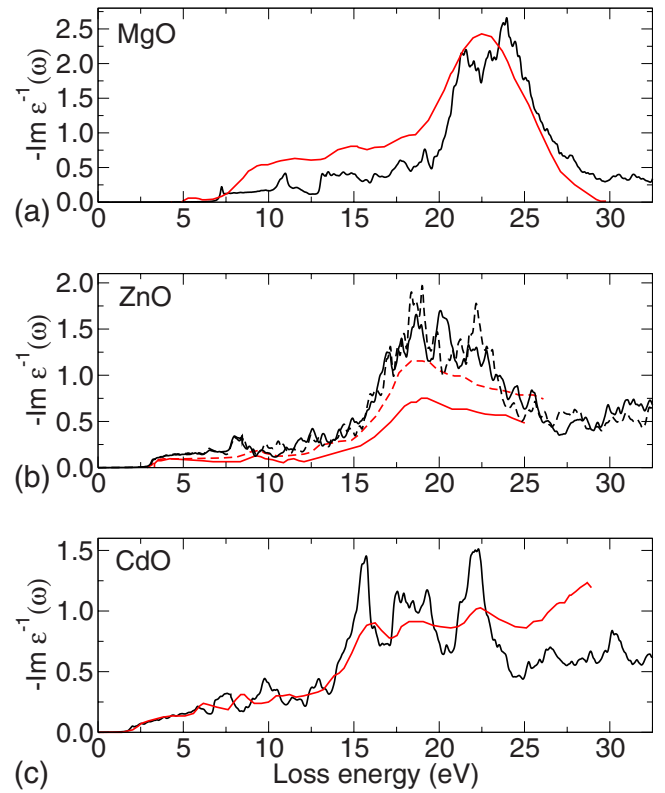


FIG. 4. (Color online) Electron-energy-loss function  $-\text{Im } \epsilon^{-1}(\omega)$  according to Eq. (2) of (a) rs-MgO, (b) wz-ZnO, and (c) rs-CdO, including excitonic effects (black curves). We compare to experimental (red/bright lines) results from Ref. 50 (MgO) and Ref. 38 (ZnO and CdO). For the hexagonal wz-ZnO curves for the ordinary direction (solid lines) as well as for the extraordinary direction (dashed lines) are shown.

parts of the dielectric function. As discussed before, we identify the two peaks at photon energies of  $\hbar\omega \approx 17$  eV and  $\hbar\omega \approx 21$  eV with transitions from the Cd  $4d$  states into the CBs. In the different reflectivity experiments<sup>38,47</sup> several peaks and shoulders are observed but with slightly varying positions and intensities. The comparison to an experimental result<sup>38</sup> yields good agreement for the peaks at energies above 10 eV as well as up to 6 eV. We are able to reproduce the peak complex at energies from 12 to 15 eV as well as the peaks around  $\hbar\omega=17.4$  eV and  $\hbar\omega=21.4$  eV. In the low-energy regime between 6 and 10 eV the agreement is worse and we find differences of about 1.2 eV between experimental and theoretical peak positions.

## B. Electron-energy-loss function

In Fig. 4 we present results for the electron-energy-loss function for the three oxides as computed from the dielectric functions  $\epsilon(\omega)$  using Eq. (2). For MgO [cf. Fig. 4(a)] we find a pronounced plasmon resonance of the  $sp$  electrons around energies of 23.8 eV. The plasma frequency of the valence electrons derived from the theoretical lattice parameters<sup>14</sup> amounts to  $\hbar\omega_p=23.9$  eV. However, the broad plasmon peak exhibits a fine structure due to the frequency behavior of the dielectric function. We can relate the peak at energies

of about 21.5 eV to the vanishing real part of the dielectric function. Also the peaks around 23 and 24 eV are due to the small absolute value of  $\text{Re } \varepsilon(\omega)$  [cf. Fig. 2(a)]. The comparison with the experimental findings by Kohiki *et al.*<sup>50</sup> shows overall good agreement. The onset is found below the gap at energies of about 5 eV in experiment, while our computed value for the edge amounts to 7.2 eV, in agreement with other measurements determining the gap. Besides these two features the experimental curve does not show much structure. Assuming a certain broadening it agrees well with our result.

For wz-ZnO we study the energy-loss functions in Fig. 4(b). We observe a small peak at energies around 8.1 eV and a broad plasma resonance around 20 eV independent of the direction. The splitting of this broad structure may be related to the successive contributions of the *p*-type, *s*- and *p*-type, and *s*-, *p*-, and *d*-type valence electrons to the plasma resonance with plasma frequencies near 18.3, 21.1, and below 31.6 eV (the *d* electrons do not contribute fully because of their stronger bonding). In any case, the absolute values of the real parts of the dielectric functions  $\text{Re } \varepsilon^{\parallel}(\omega)$  and  $\text{Re } \varepsilon^{\perp}(\omega)$  are small in the region between 14 and 21 eV with a zero at around 17 eV. Besides, in the energy range between 18 and 23 eV the anisotropy we find remains small. The comparison to experimental results<sup>38</sup> shows good agreement for the overall line shape. The peak structure which is found here with energies of about 8.1 eV occurs roughly at 9.4 eV in experiment. As discussed in Sec. IV, this might be attributed to the use of a scissor operator, which leads to an underestimation of the energetic positions of the high-energy optical transitions. On the other hand, we can identify peaks around energies of 18.7 eV with structures in the experimental curve. We do not confirm the remarkable anisotropy found experimentally in Ref. 38. However, other experimental results for the electron-energy-loss function of ZnO computed by a Kramers-Kronig analysis<sup>36,47</sup> agree much better with our result and exhibit a much weaker anisotropy than the one given in Ref. 38.

The electron-energy-loss curve for rs-CdO is shown in Fig. 4(c). As already stated for the reflectivity, also the loss function represents many of the features of the imaginary part of the dielectric function. We do not find one single pronounced plasma resonance of the *sp* or *d* electrons. Instead, Fig. 4(c) shows a clear three-peak structure at energies between 15 and 23 eV. The plasma frequency of the *sp* electrons amounts to approximately  $\hbar\omega=20.1$  eV. Test calculations using the RPA spectrum lead us to the conclusion that

at least parts of the three-peak structure are due to the presence of the Cd 4*d* electrons and the corresponding peaks in the dielectric function. We did not find such a clear assignment for wz-ZnO, possibly a consequence of the Zn 3*d* states being slightly less separated from the O 2*p* states. The peak around energies of about 15.5 eV in the spectrum of CdO correlates with the vanishing real part of the dielectric function. The observed three-peak structure is confirmed by the measured spectrum.<sup>38</sup> With respect to the experimental result, we underestimate the peak positions by about 0.5–1.0 eV for reasons discussed above.

## VI. CONCLUSIONS

In conclusion, using many-body *ab initio* methods and quasiparticle electronic structures we have computed the dielectric function, the reflectivity, and the electron-energy-loss function of rs-MgO, wz-ZnO, and rs-CdO in a wide spectral range. We justified the used GGA+*U*+ $\Delta$  approach by detailed comparison to results for the band structures and DOS obtained within the HSE03+*GW* scheme.

The calculated dielectric functions including excitonic and LFEs are extensively compared to experimental results for MgO, ZnO, and CdO. We obtain convincing agreement and are able to explain relevant peaks in the absorption spectrum by optical interband transitions as well as their shift and mixing by many-body effects. The influence of the shallow semicore *d* electrons has been explicitly pointed out and also the consequences of excitonic effects have been discussed in detail. In addition, we have compared the obtained reflectivity and the energy-loss functions of the three oxides with experimental curves and discussed the observed features in terms of band structures and plasmon effects.

By comparing the dielectric functions for all three oxides, trends for peak positions and peak heights have been discussed along the chemical row MgO, ZnO, and CdO.

## ACKNOWLEDGMENTS

Helpful discussions with Olivia Pulci, Munise Rakel, Paola Gori, Christoph Cobet, and Rüdiger Goldhahn are gratefully acknowledged. Furthermore, this work was supported by the Carl-Zeiss-Stiftung, the Deutsche Forschungsgemeinschaft (Project No. Be1346/20-1), the BMBF Germany (Project No. 13N9669), and the European Community in the framework of the ETSF (Grant No. 211956). Further, we thank the LRZ Munich and HLR Stuttgart for computing time.

<sup>1</sup>M. Joseph, H. Tabata, and T. Kawai, Jpn. J. Appl. Phys., Part 2 **38**, L1205 (1999).

<sup>2</sup>Ü. Özgür, Ya. I. Alivov, C. Liu, A. Teke, M. A. Reshchikov, S. Doğan, V. Avrutin, S.-J. Cho, and H. Morkoç, J. Appl. Phys. **98**, 041301 (2005).

<sup>3</sup>L. Schmidt-Mende and J. L. MacManus-Driscoll, Mater. Today **10**, 40 (2007).

<sup>4</sup>A. Ohtomo and A. Tsukazaki, Semicond. Sci. Technol. **20**, S1

(2005).

<sup>5</sup>S. Sadofev, S. Blumstengel, J. Cui, J. Puls, S. Rogaschewski, P. Schäfer, Y. G. Sadofyev, and F. Henneberger, Appl. Phys. Lett. **87**, 091903 (2005).

<sup>6</sup>S. Sadofev, S. Blumstengel, J. Cui, J. Puls, S. Rogaschewski, P. Schäfer, and F. Henneberger, Appl. Phys. Lett. **89**, 201907 (2006).

<sup>7</sup>S. Shigemori, A. Nakamura, J. Ishihara, T. Aoki, and J. Temmyo,

- Jpn. J. Appl. Phys., Part 2 **43**, L1088 (2004).
- <sup>8</sup>A. Tsukazaki, A. Ohtomo, T. Kita, Y. Ohno, H. Ohno, and M. Kawasaki, *Science* **315**, 1388 (2007).
- <sup>9</sup>W. G. Aulbur, L. Jönsson, and J. W. Wilkins, *Solid State Physics: Advances in Research and Applications* (Academic, San Diego, 2000), Vol. 54, p. 1.
- <sup>10</sup>L. Hedin, *Phys. Rev.* **139**, A796 (1965).
- <sup>11</sup>W. Kohn and L. J. Sham, *Phys. Rev.* **140**, A1133 (1965).
- <sup>12</sup>F. Fuchs, J. Furthmüller, F. Bechstedt, M. Shishkin, and G. Kresse, *Phys. Rev. B* **76**, 115109 (2007).
- <sup>13</sup>P. Rinke, A. Qteish, J. Neugebauer, and M. Scheffler, *Phys. Status Solidi B* **245**, 929 (2008).
- <sup>14</sup>A. Schleife, F. Fuchs, J. Furthmüller, and F. Bechstedt, *Phys. Rev. B* **73**, 245212 (2006).
- <sup>15</sup>C. Rödl, F. Fuchs, J. Furthmüller, and F. Bechstedt, *Phys. Rev. B* **77**, 184408 (2008).
- <sup>16</sup>C. Rödl, F. Fuchs, J. Furthmüller, and F. Bechstedt, *Phys. Rev. B* **79**, 235114 (2009).
- <sup>17</sup>A. Schleife *et al.*, *J. Korean Phys. Soc.* **53**, 2811 (2008).
- <sup>18</sup>J. Heyd, G. E. Scuseria, and M. Ernzerhof, *J. Chem. Phys.* **118**, 8207 (2003).
- <sup>19</sup>A. R. H. Preston, B. J. Ruck, L. F. J. Piper, A. DeMasi, K. E. Smith, A. Schleife, F. Fuchs, F. Bechstedt, J. Chai, and S. M. Durbin, *Phys. Rev. B* **78**, 155114 (2008).
- <sup>20</sup>L. F. J. Piper, A. DeMasi, K. E. Smith, A. Schleife, F. Fuchs, F. Bechstedt, J. Zúñiga-Pérez, and V. Muñoz-Sanjosé, *Phys. Rev. B* **77**, 125204 (2008).
- <sup>21</sup>L. F. J. Piper *et al.*, *Phys. Rev. B* **78**, 165127 (2008).
- <sup>22</sup>J. P. Perdew, in *Electronic Structure of Solids '91*, edited by P. Ziesche and H. Eschrig (Akademie-Verlag, Berlin, 1991), p. 11.
- <sup>23</sup>V. I. Anisimov, J. Zaanen, and O. K. Andersen, *Phys. Rev. B* **44**, 943 (1991).
- <sup>24</sup>S. L. Dudarev, G. A. Botton, S. Y. Savrasov, C. J. Humphreys, and A. P. Sutton, *Phys. Rev. B* **57**, 1505 (1998).
- <sup>25</sup>W. Hanke and L. J. Sham, *Phys. Rev. Lett.* **43**, 387 (1979).
- <sup>26</sup>G. Strinati, *Riv. Nuovo Cimento* **11**, 1 (1988).
- <sup>27</sup>S. Albrecht, L. Reining, R. Del Sole, and G. Onida, *Phys. Rev. Lett.* **80**, 4510 (1998).
- <sup>28</sup>L. X. Benedict, E. L. Shirley, and R. B. Bohn, *Phys. Rev. Lett.* **80**, 4514 (1998).
- <sup>29</sup>M. Rohlfiing and S. G. Louie, *Phys. Rev. Lett.* **81**, 2312 (1998).
- <sup>30</sup>F. Fuchs, C. Rödl, A. Schleife, and F. Bechstedt, *Phys. Rev. B* **78**, 085103 (2008).
- <sup>31</sup>B. Adolph, V. I. Gavrilenko, K. Tenelsen, F. Bechstedt, and R. Del Sole, *Phys. Rev. B* **53**, 9797 (1996).
- <sup>32</sup>H. J. Monkhorst and J. D. Pack, *Phys. Rev. B* **13**, 5188 (1976).
- <sup>33</sup>W. G. Schmidt, S. Glutsch, P. H. Hahn, and F. Bechstedt, *Phys. Rev. B* **67**, 085307 (2003).
- <sup>34</sup>G. Kresse and D. Joubert, *Phys. Rev. B* **59**, 1758 (1999).
- <sup>35</sup>*Springer Handbook of Condensed Matter and Materials Data*, edited by W. Martienssen and H. Warlimont (Springer-Verlag, Berlin, 2005).
- <sup>36</sup>M. Rakel, C. Cobet, N. Esser, P. Gori, O. Pulci, A. Seitsonen, A. Cricenti, N. Nickel, and W. Richter, *Epioptics-9* (World Scientific, Singapore, 2008).
- <sup>37</sup>M. L. Bortz, R. H. French, D. J. Jones, R. V. Kasowski, and F. S. Ohuchi, *Phys. Scr.* **41**, 537 (1990).
- <sup>38</sup>J. L. Freeouf, *Phys. Rev. B* **7**, 3810 (1973).
- <sup>39</sup>H. Ehrenreich and M. H. Cohen, *Phys. Rev.* **115**, 786 (1959).
- <sup>40</sup>R. Schmidt-Grund, B. Rheinländer, E. M. Kaidashev, M. Lorenz, M. Grundmann, D. Fritsch, M. M. Schubert, H. Schmidt, and C. M. Herzinger, *J. Korean Phys. Soc.* **53**, 88 (2008).
- <sup>41</sup>M. Gajdoš, K. Hummer, G. Kresse, J. Furthmüller, and F. Bechstedt, *Phys. Rev. B* **73**, 045112 (2006).
- <sup>42</sup>M. W. Williams and E. T. Arakawa, *J. Appl. Phys.* **38**, 5272 (1967).
- <sup>43</sup>D. M. Roessler and W. C. Walker, *Phys. Rev.* **159**, 733 (1967).
- <sup>44</sup>N.-P. Wang, M. Rohlfiing, P. Krüger, and J. Pollmann, *Appl. Phys. A: Mater. Sci. Process.* **78**, 213 (2004).
- <sup>45</sup>A. Schleife, C. Rödl, F. Fuchs, J. Furthmüller, and F. Bechstedt, *Appl. Phys. Lett.* **91**, 241915 (2007).
- <sup>46</sup>R. Laskowski and N. E. Christensen, *Phys. Rev. B* **73**, 045201 (2006).
- <sup>47</sup>R. Klucker, H. Nelkowski, Y. S. Park, M. Skibowski, and T. S. Wagner, *Phys. Status Solidi B* **45**, 265 (1971).
- <sup>48</sup>W. R. L. Lambrecht, B. Segall, J. Rife, W. R. Hunter, and D. K. Wickenden, *Phys. Rev. B* **51**, 13516 (1995).
- <sup>49</sup>W. R. L. Lambrecht and M. Prikhodko, *Solid State Commun.* **121**, 549 (2002).
- <sup>50</sup>S. Kohiki, M. Arai, H. Yoshikawa, and S. Fukushima, *J. Phys. Chem. B* **103**, 5296 (1999).